Available online at www.sciencedirect.com
SCIENCE DIRECT
Polymer 46 (2005) 7370–7385
polymer
www.elsevier.com/locate/polymer

Deformation and damage upon stretching of degradable polymers (PLA and PCL)

F. Rezgui[1], M. Swistek, J.M. Hiver, C. G'Sell*, T. Sadoun[1]

Laboratoire de Physique des Matériaux (UMR CNRS 7556), Ecole des Mines de Nancy (INPL), Parc de Saurupt, 54042 Nancy, France

Received 11 December 2004; received in revised form 1 March 2005; accepted 11 March 2005
Available online 11 July 2005

Abstract

Microstructure and plastic behavior of poly(lactic acid), PLA, and poly(ε-caprolactone), PCL, are investigated. The injected molded specimens are analyzed as received. Thermomechanical properties are characterized by DSC and DMA and crystalline structure by WAXS. The results show that PLA samples are weakly crystalline (14 wt%) and that amorphous phase is glassy at room temperature. The PCL samples exhibit higher crystallinity (53 wt%) and contain a rubber-like amorphous phase. Mechanical behavior is investigated by means of novel video-controlled materials testing system specially developed to assess true stress vs. true strain curves and to record the volume changes upon stretching. While tested at 50 °C, PLA undergoes extensive plastic deformation with a dramatic yield softening followed by a progressively increasing strain hardening. Volume strain, which characterizes deformation damage, increases steadily over the whole plastic stage until reaching 0.27 for an axial strain of 1, 4. For its part, PCL exhibits at 23 °C a much progressive plastic response with a soft yield point, no softening, and moderate strain hardening at large strain. Volume change is delayed until axial strain reaches 0.4. Subsequent damage grows very quickly, eventually reaching 0.2 for an ultimate strain of 1, 3. Results are discussed on the basis of microscopic damage mechanisms observed in the stretched state.

Keywords: Degradable polymers; PLA; PCL

1. Introduction

Although degradable polymers occupy a very marginal position among structural materials in the present state of the market, they will probably know significant progress in the next decade. The first application concerns packaging materials (bags, films, wrappers, containers, etc.) that are a major source of plastic wastes and for which utilization of degradable polymers potentially constitutes, at least partially, a valuable solution for the serious environmental problems encountered presently [1]. Another, more technical, application is related to medical technologies. The synthetic materials used in this field range from common products such as sutures to elaborate products such as scaffolds for tissue engineering.

Among others, two polyesters are serious candidate for such development: poly(lactic acid), PLA for short, and poly(ε-caprolactone), PCL. These polymers degrade by hydrolytic or enzymatic pathways, making them suitable for packaging and medical uses [2–8].

PLA is a linear aliphatic thermoplastic polyester, produced from renewable resources and readily biodegradable. It is produced by ring-opening polymerization of lactides and the lactic acid monomer used are obtained from the fermentations of sugar feedstocks [9]. Generally, commercial PLA grades are copolymers of poly(L-lactic acid), noted PLLA, and poly(D,L-lactic acid), noted PDLLA, which are produced from L-lactides and D,L-lactides, respectively. The ratio of L- to D,L-enantiomers is known to affect the properties of the polymer obtained, such as melting temperature and degree of crystallinity [10].

PCL is another aliphatic polyester, but this one is obtained through petrochemical processes. Nevertheless, it is degradable in several biotic environments, including river

* Corresponding author. Tel.: +33 3 83 58 41 54; fax: +33 3 83 57 97 94.
E-mail address: gsell@mines.inpl-nancy.fr (C. G'Sell).
[1] Permanent address: Laboratoire des Matériaux Organiques, Département de Génie des Procédés, Faculté des Sciences et Sciences de l'Ingénieur, Université de Bejaia, Route de Targa ouzemour, 06000 Bejaia, Algérie.

0032-3861/$ - see front matter © 2005 Elsevier Ltd. All rights reserved.
doi:10.1016/j.polymer.2005.03.116

and lake waters, sewage sludge, farm or paddy soil, compost and various sediments. Furthermore, it is non-toxic versus biological tissues. PCL is therefore suitable for many uses, providing its mechanical and environmental properties are adapted. Particularly, it has been shown that molecular weight and crystallinity have important effect on its biodegradability [4]. Also, PCL has interesting compatibility with various polymers, making possible the preparation of blends [1,5,7,10].

The aim of this paper is to present preliminary results obtained in a more general work devoted to the design of degradable materials for structural and/or functional applications. More specifically, we aim to characterize and model the influence of formulation and processing on the mechanical and environmental properties of blends and composites based on PLA and PCL. In this first publication, the interest is focused on the stretching capability of neat grades of both polymers. Firstly, the microstructure of the materials will be carefully analyzed by means of several complementary techniques including differential scanning calorimetry (DSC), dynamic mechanical analysis (DMA), wide-angle X-ray scattering (WAXS) and scanning electron microscopy (SEM). Subsequently, the constitutive behavior of PLA and PCL up to large strains under uniaxial tension will be determined by means of a novel video-controlled tensile testing method. As we will see below, this method gives access not only to the plastic response through the true stress–strain relation, but also to the intrinsic damage processes through the evolution of volume strain.

2. Experimental

2.1. Materials and sample preparation

The PLA under investigation in this work is a neat grade commercialized by Cargill-Dow under the brand name 'NatureWorks 3001D'. Its composition is close to the one previously studied by Avérous [10] that consists in 92% L-lactide and 8% *meso*-lactide. The role of the latter isomer, in addition to the L-lactide, is to limit crystallinity and hence promote higher toughness. The distribution of molecular weight was performed with a Waters GPC system (Model 2695) operating with chloroform in polymer labs columns. The number- and weight-average molecular weight thus obtained are equal to 107,000 and 152,000 g/mol, respectively. The viscosity-average molecular weight, indicated by Cargill-Dow, is equal to 150.000 g/mol. The melt flow index (MFI) is in the range from 10 to 30 g/10 min (temperature 190 °C, pressing mass 2.16 kg). The density of the pellets is equal to 1.21 g/cm^3.

The PCL is polymerized from ε-caprolactone. The material utilized here is a neat grade provided by Solvay (brand name 'Capa 680'). The number- and weight-average molecular weight, measured by GPC at Solvay laboratories (Brussels) are 70,000 and 123,000 g/mol, respectively. The MFI, measured in the same conditions as for PLA, is equal to 7.3 g/10 min. The density is equal to 1.2 g/cm^3.

PLA and PCL pellets were carefully desiccated for 12 h in a vacuum oven at 50 °C. Subsequently, the plates of 4 mm thickness were molded in a Sandretto hydraulic press (model Euromap 310/95, screw diameter 45 mm). Injection molding conditions for PLA are: temperature profile, 165–205 °C; injection pressure, 80 bar; screw speed, 150 rpm. The conditions used for PCL are: temperature profile, 130–180 °C; injection pressure, 90 bar; screw speed, 150 rpm.

2.2. Thermomechanical analysis

Thermal analysis was performed by means of a Perkin–Elmer differential scanning calorimeter (DSC 7). The samples were sealed in aluminum pans (8 mg) and heated from 20 to 180 °C at a rate of 10 °C/min. They were cooled back to 20 °C at a rate of 200 °C/min. The glass transition temperature, T_g, was measured at the mid-point of the heat capacity inflexion point. As for the crystallization temperature, T_c, and melting temperature, T_m, they were determined from the peak value of the respective endotherms and exotherms. The degree of crystallinity of samples, χ_c, was calculated by the conventional 2-phase approximation as $\chi_c = \Delta H_m/\Delta H_m^0$, where ΔH_m is the measured enthalpy of melting and ΔH_m^0 the enthalpy of melting of 100% crystalline polymer (93 J/g for PLA [10] and 136 J/g for PCL [11]).

Dynamic mechanical analysis (DMA) was carried out with a Netsch equipment (DMA 242 C). Test bars were cut from the injected plates (dimensions $L\times W\times H = 60\times 10\times 4$ mm^3) and mounted on a dual-cantilever bending rig. The temperature used in the experiments ranged from −150 to +150 °C for PLA and from −150 to +50 °C for PCL, at a heating rate of 2 °C/min. The deflection was set at 50 μm, and four frequencies were used, ranging from 1 to 25 Hz. The viscoelastic properties were characterized versus temperature and frequency, namely the storage modulus, E', the loss modulus, E'', and the mechanical loss factor, $\tan\delta = E''/E'$. The activation energies of the observed transitions were calculated from the temperature/frequency relationship.

2.3. Microstructural characterization

Wide-angle X-ray scattering (WAXS) was used to probe the crystalline structure of polymers. The cylindrical incident beam are obtained from a X-ray tube with a graphite mirror ($\lambda_{Cu\ K\alpha} = 0.154$ nm) and a very fine capillary (diameter 0.35 mm). The diffraction patterns are analyzed by means of a horizontal camera equipped with a curved detector covering 120° diffraction angles in fixed position (Inel, France). The samples are parallelepipedic with a thickness of about 0.5 mm.

Defects in the deformed materials were examined using a scanning electron microscope (SEM: Philips field emission

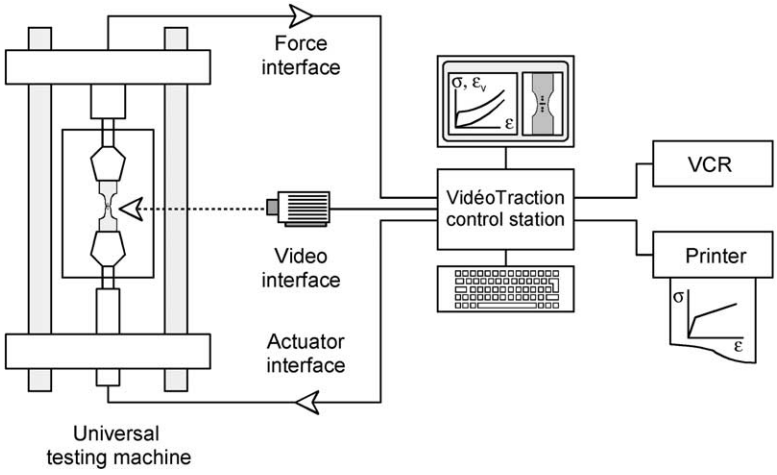

Fig. 1. General diagram of the VidéoTraction© system.

gun 30 XLS operating at 2 keV in secondary emission mode). Prior to stretching, the tensile samples were finely polishing with successively finer abrasive (finishing with 1 μm diameter alumina powder) in such a way that no significant scratch or pit was left on the surface. After stretching, the samples were coated with a thin layer of gold and observed in the SEM.

2.4. Video-controlled tensile testing

The video-controlled materials testing system (Vidéo-Traction©, Apollor, Vandoeuvre) has already been described elsewhere [12]. This technique (Fig. 1) is based on the measurement and regulation of the local deformation in a representative volume element (RVE) by means of an intelligent optical extensometer. Dot markers are printed on the tensile specimens with black ink specially prepared to adhere correctly on the sample without damaging the polymer. A digital video camera analyzes their relative displacements during the course of the test. A thermally controlled chamber keeps the temperature constant and protects the sample from the thermal radiation the marker illuminator. Mechanical data analysis (stress, strain, volume strain) is performed in real time, while the axial strain is dynamically regulated at a constant rate.

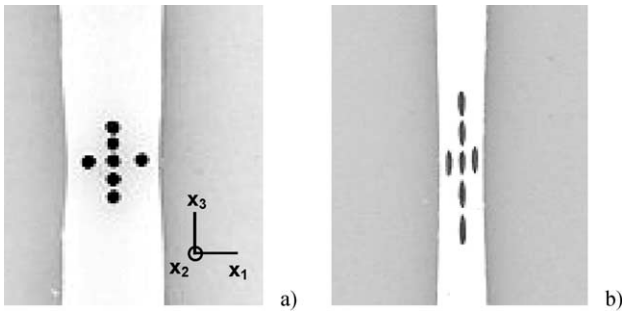

Fig. 2. Configuration of the seven markers on a PLA sample (a) before stretching and, (b) deformed to a true axial strain $\varepsilon_{33} = 1.4$ at a temperature of 50 °C.

For the video-controlled tests, the samples are prepared in the following way. Parallelepipeds ($100 \times 10 \times 4$ mm^3) are carefully machined out of the molded plates by means of a computerized milling machine (CharlyRobot). In order to localize the deformation in the RVE where all the mechanical variables are determined, a geometric defect is machined in the center of the specimens, were the local width is reduced from 8 to 5.5 mm over a length of 5 mm. The disposition of the ink markers is illustrated in Fig. 2(a). The five markers aligned along the tensile axis, x_3, are printed with center-to-center distances of about 1 mm. The three markers aligned along the transversal axis, x_1, are more widely separated, in such a way that they occupy a major fraction of the total width in the geometric defect. The diagram in Fig. 2(b) is a macrograph of a PLA sample showing the configuration of the seven markers after some amount of deformation. The aim of the method is to determine properly the three principal components of strain, ε_{11}, ε_{22}, ε_{33}, together with the true stress, σ_{33}, in the representative volume element (RVE) constituted by a slice of material across the sample at the level of the three transverse markers, where stresses and strains should be nearly uniform. Since, the alignment of these dots perpendicularly to the tensile axis is not perfect, the RVE is not ideally thin in the x_3 direction, its thickness being of the order of 0.2 mm.

Lets us consider first the axial strain distribution. Average strain between adjacent markers is obtained following the 'true' (or 'natural') definition of Hencky by relations of the type: $\varepsilon_{33}(x_{3i}) = \ln(L_{3i}/L^0_{3i})$, where L^0_{3i} and L_{3i} ($i = 1$ to 4) are the initial and current distances of the centers of gravity of the ith close pair of markers aligned along the x_3 axis, and x_{3i} is the median coordinate of the marker pair, to which this strain value is ascribed. The axial true strain in the RVE, ε_{33}, is obtained by adequate interpolation of the four ε_{33} (x_{3i}) values at the central coordinate of the RVE.

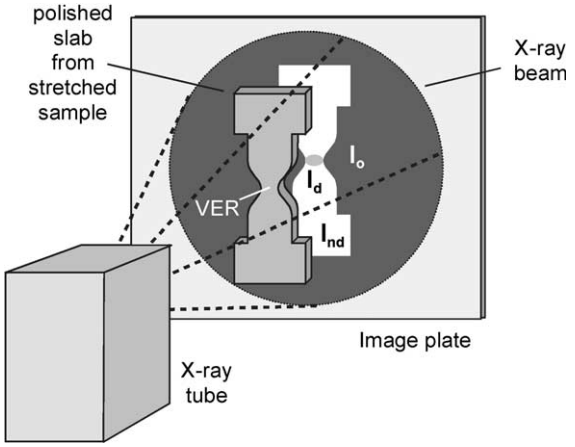

Fig. 3. Schematic diagram of the X-ray radiographic setup for assessment of volume strain. Note: for clarity, the sample has been drawn detached from the image plate, while in reality, it is pressed onto the plate.

Subsequently, we define the transverse true strain in the RVE, ε_{11}, from the relative positions of the two exterior markers in the set of three printed along the x_1 axis. This is done by using the same Hencky expression as before: $\varepsilon_{11} = \ln(L_1/L_1^0)$, where L_1^0 and L_1 are the initial and current distances (along x_1) of the centers of gravity of the two markers under consideration.

Lastly, we consider by the virtue of the transverse isotropy that both transverse strains are equal, that is: $\varepsilon_{22} = \varepsilon_{11}$. That property was carefully verified in reference specimens by measuring the local width and thickness at the level of the RVE by means of a precision caliper.

Since, the three components of strain are defined in the same RVE, the trace of the tensor can be calculated. It is called 'volume strain' since it measures the dilatation (or contraction of the RVE: $\varepsilon_v = \varepsilon_{11} + \varepsilon_{22} + \varepsilon_{33} = \ln(V/V_0)$). The final precision on the determination of volume strain is equal to about 10^{-3}.

The appropriate stress definition associated with the Hencky strain is the Cauchy stress (also called 'true' stress). It takes into account the reduction of the cross-sectional

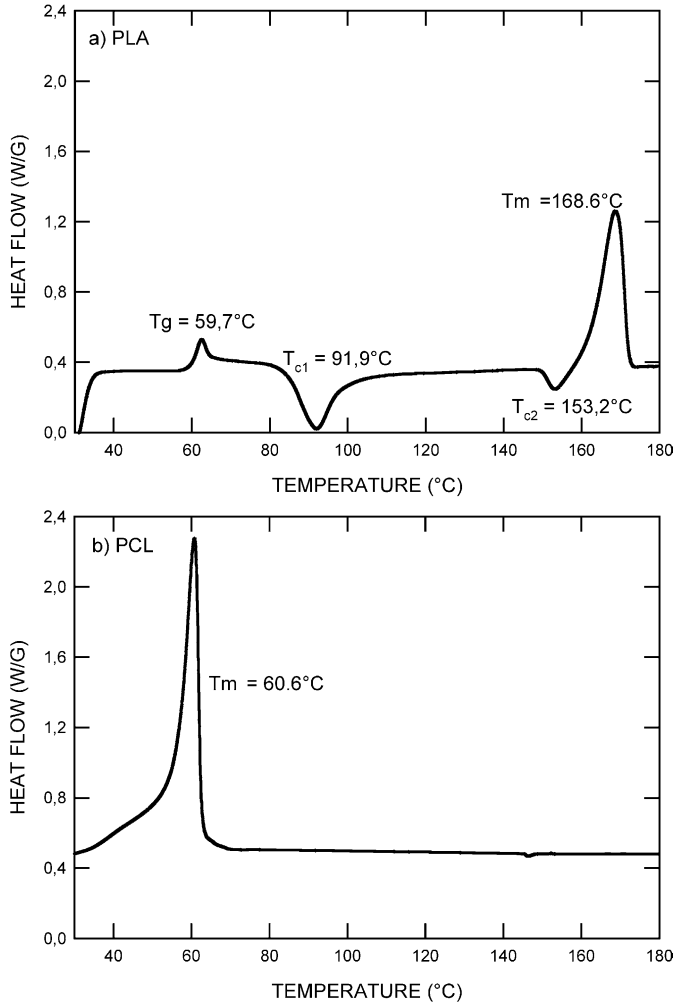

Fig. 4. DSC thermograms for (a) PLA and (b) PCL.

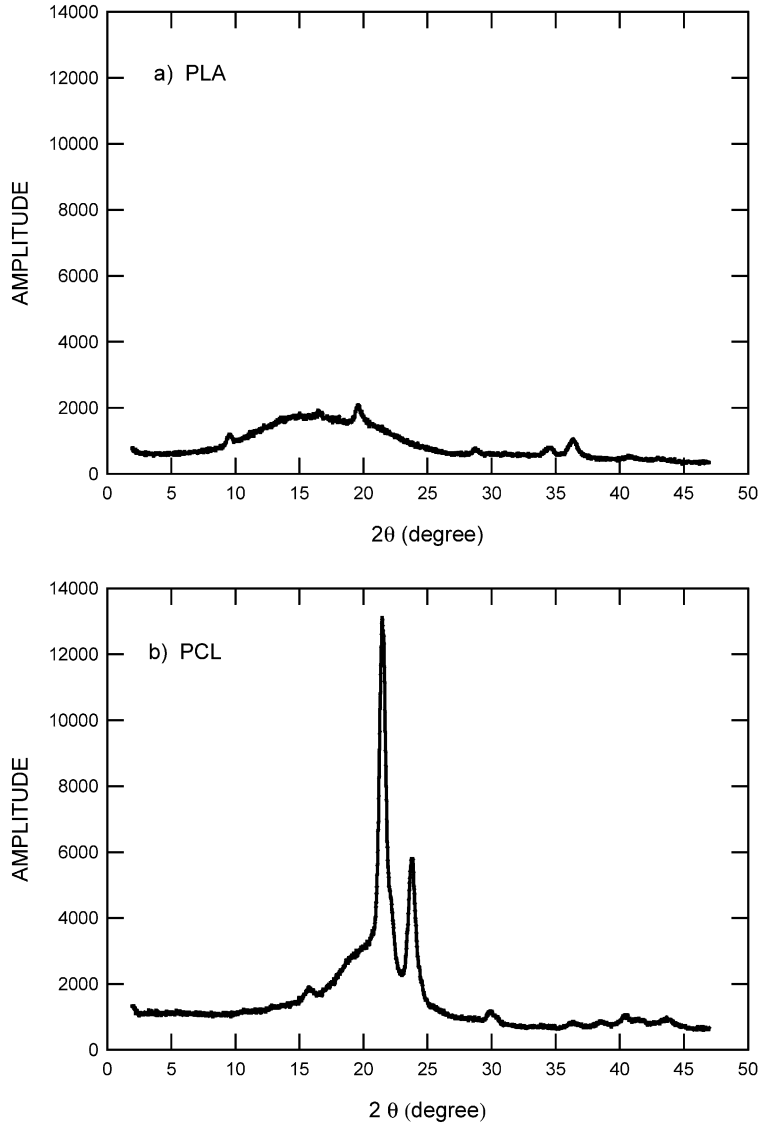

Fig. 5. X-ray diffraction profiles (WAXS) for (a) PLA and (b) PCL.

area, $A<A_0$, undergone by the specimen while it is stretched: $\sigma_{33}=F/A=(F/A_0)\exp(-\varepsilon_{11}-\varepsilon_{22})$.

2.5. X-ray densitometry

X-ray densitometry is used in this work to quantify deformation damage in polymers after stretching. This technique, intrinsically non destructive, is based on the same principles as in medical radiography. Each deformed sample is first polished on both front and rear faces until obtaining a slab of uniform thickness slightly lower than that of the central zone of the neck, where the RVE is located. Subsequently, the sample is placed in the beam generated by an X-ray tube equipped with a tungsten anode and set at 10 kV and 1 mA (Inel XRG 3000). As shown in Fig. 3, the X-ray intensity transmitted through the sample is recorded by means of a high-resolution image plate sensitive to X-ray photons (IP Fujifilm). The two-dimensional radiographic image is revealed with the appropriate reader (Fujifilm BAS-5000). Classical Beer–Lambert's law states that the distribution of transmitted intensity is given by $I(x_1, x_3)=I_0\exp(-\mu(x_1, x_3)t)$, where I_0 is the incident beam intensity, t the thickness of the slab (that is uniform after polishing) and $\mu(x_1, x_3)$ the average through-thickness absorption coefficient at each point of (x_1, x_3) coordinates. For a sample damaged by plastic deformation, the absorption coefficient at the RVE is given by $\mu(x_1, x_3)=\mu_0(\rho_{nd}/\rho_d)$; in this equation, ρ_{nd} is the density of the non-deformed polymer (outside the calibrated zone of the sample) and ρ_d the average through-thickness density at the RVE. Since, volume strain measures the local density loss one gets $\varepsilon_v=\ln(v_d/v_{nd})=\ln(\rho_{nd}/\rho_d)$. Consequently, ε_v is readily obtained from the recorded map of transmitted X-ray intensity by the relation: $\varepsilon_v=\ln[\ln(I_0/I_{nd})]-\ln[\ln(I_0/I_d)]$. Here, I_0, I_{nd} and I_d are

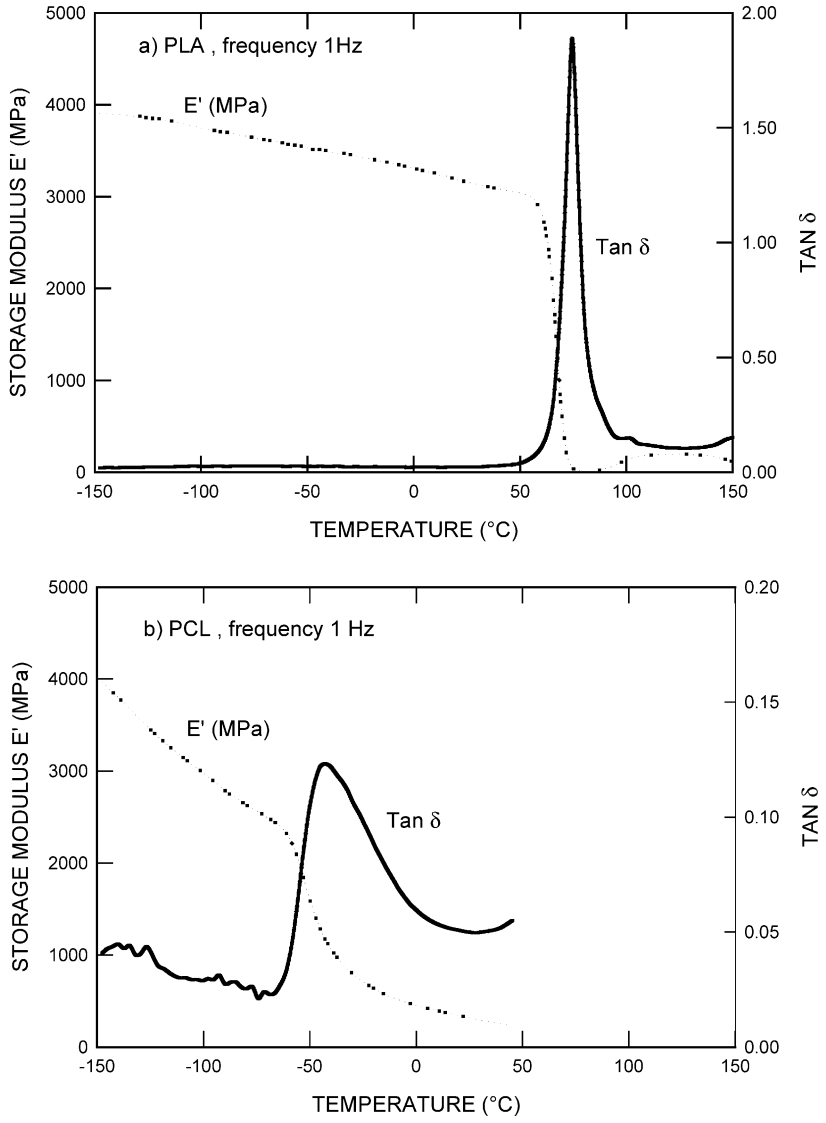

Fig. 6. Storage modulus (E') and loss factor (tan δ) obtained by DMA at 1 Hz for (a) PLA and (b) PCL.

measured outside the sample, in the non-deformed part of the sample and in the VRE, respectively.

2.6. Electron microscopy

Occurrence of deformation damage was investigated in PLA and PCL specimens by means of a scanning electron microscope (SEM) equipped with a field-effect gun (Philips FEG XL 30). Before stretching, specimens were carefully polished with fine sand paper and diamond paste until no major defects were still visible. Subsequently, specimens were stretched with the VidéoTraction© system at a strain rate of about $10^{-3}\,s^{-1}$ until an axial true train $\varepsilon_{33} \approx 1.4$ was attained in the RVE. Lastly, the specimens were introduced in the SEM chamber for observing their surface through secondary electron detector. No etching treatment was used in this protocol in order to avoid surface perturbation.

3. Microstructural characterization of the undeformed polymers

3.1. Thermal analysis

The results obtained from differential scanning calorimetry of PLA and PCL are displayed in Fig. 4. The PLA thermogram shows several features: (i) a clear glass transition at $T_g = 59.7\,^{\circ}C$, (ii) two crystallization peaks situated at $T_{c1} = 91.9\,^{\circ}C$ and $T_{c2} = 153.2\,^{\circ}C$, respectively, and, (iii) a large melting peak at $T_m = 168.6\,^{\circ}C$. The two crystallization peaks correspond to the two crystalline modifications of PLA, respectively, orthorhombic (β) and pseudo-orthorhombic (α) structures that have been described by Hoogsteen et al. [13]. By subtracting the two crystallization enthalpies from the heat of fusion, one finds that the degree of crystallinity in the PLA specimens is

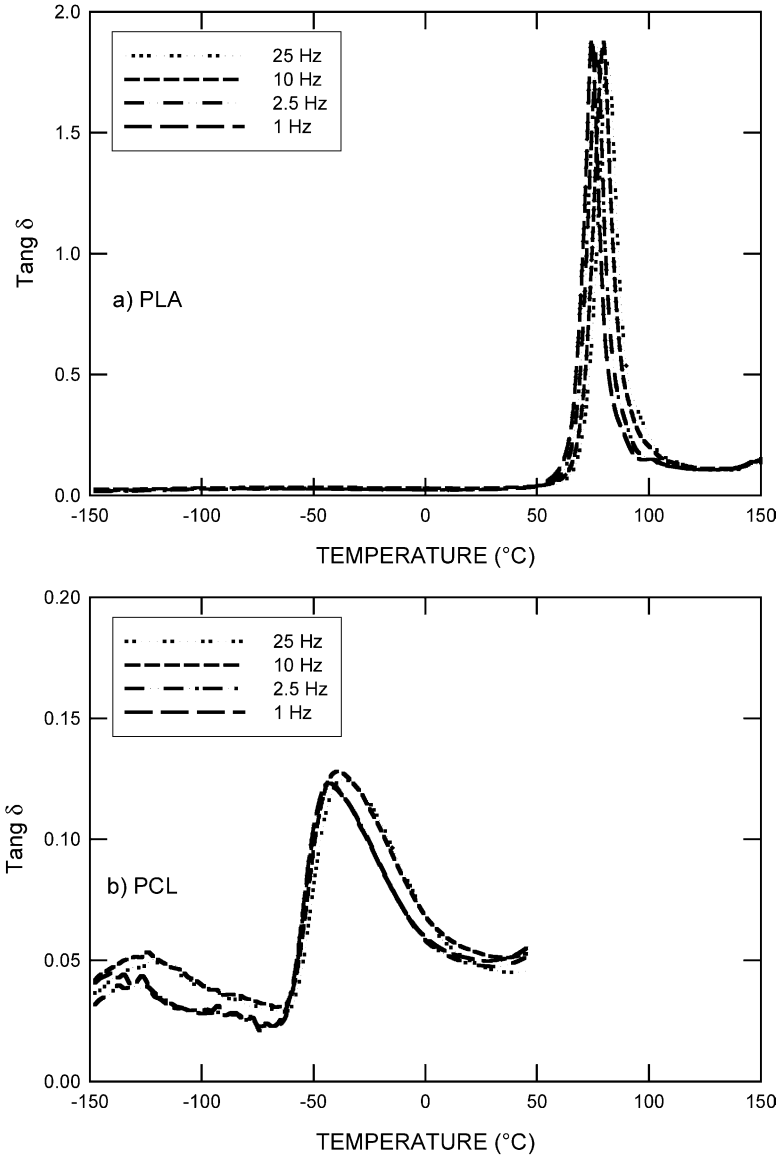

Fig. 7. DMA loss factor (tan δ) at different frequencies for (a) PLA and (b) PCL.

rather low: $\chi_c = 14.3$ wt%. The shape of the PCL thermograms is very different. We observe solely the melting peak at $T_m = 60.6$ °C. The glass transition at $T_g = -61.5$ °C, reported elsewhere [14], is outside the temperature range, and no crystallization peak is recorded. The relatively higher degree of crystallinity in PCL, $\chi_c = 53.1$ wt%, agrees with the result obtained previously by Avella et al. [11].

The DSC experiments were repeated with several specimens cut out from surface zones and from the interior of the injected plates. It was found from this investigation that the samples under are not significantly affected by the 'skin-core' effect sometimes encountered in semi-crystalline polymers due to the cooling rate gradient during the last sequence of the injection process. In particular, the index of crystallinity or the specimen is nearly constant throughout the volume.

3.2. X-ray diffraction analysis

The diffraction profiles obtained by WAXS with PLA (Fig. 5(a)) shows essentially a broad diffusion band characteristic of the amorphous phase and small crystalline peaks at $2\theta = 9.55$, 16.53, 19.65, 28.75, 34.53 and 36.38°, in agreement with previous papers [3,6,15]. Consequently, the degree of crystallinity obtained with this technique, $\chi_c = 8.3$ wt%, is not too far from the value obtained for calorimetric data, the discrepancy being due to simplifying assumptions in both methods, namely: (i) simple crystallization/melting balance for DSC and, (ii) perfect crystalline

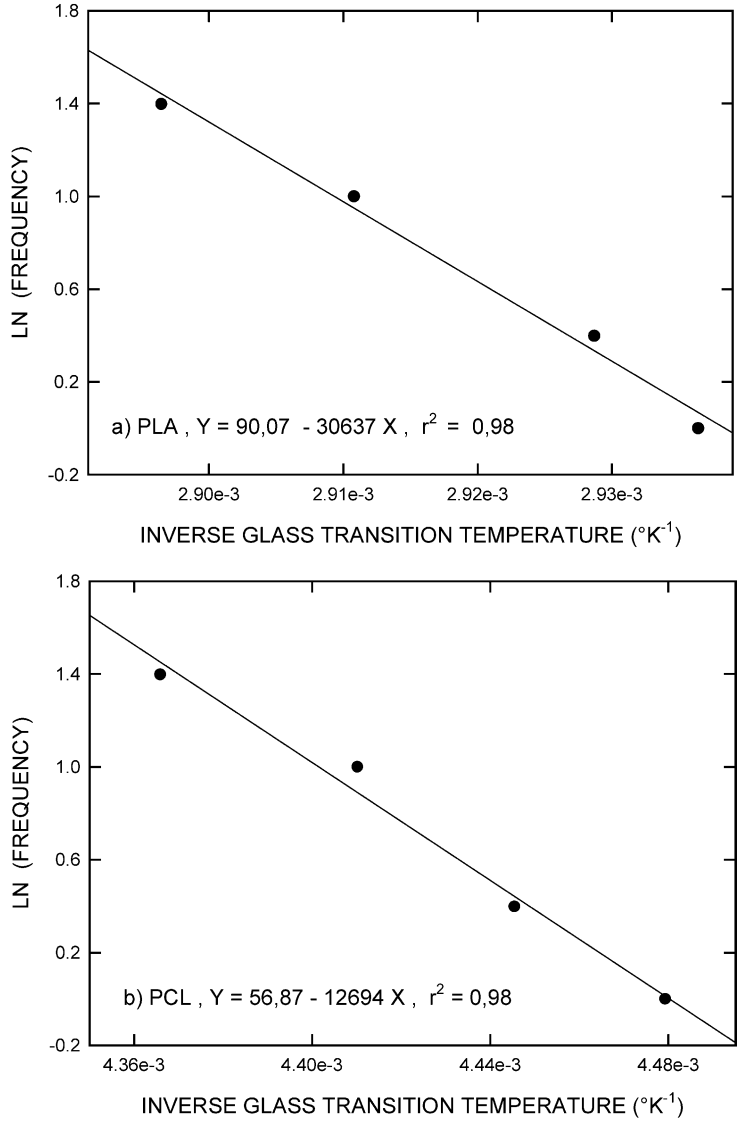

Fig. 8. Assessment of the activation energies of glass transition for (a) PLA and (b) PCL.

order for WAXS [6,16]. For PCL (Fig. 5(b)) the crystalline peaks (at $2\theta = 15.73$, 21.46, 21.62, 23.84 and 29.86°) are much more intense than for PLA, and the degree of crystallinity obtained from the deconvolution of the profile is $\chi_c = 60.5$ wt%. Such high crystallinity of PCL was previously reported by several authors [5,11,17].

3.3. DMA measurements

The influence of temperature on storage modulus, E', and loss factor, tan δ, are now presented for both materials. For PLA (Fig. 6(a)) the glass transition is clearly visible by the drop of E' and markedly by the tan δ peak at $T_g = 74$ °C. This result is not far from the value $T_g = 67$ °C obtained previously by Martin and Avérous [10] under slightly different conditions. For PCL (Fig. 6(b)) the tan δ peak is much wider and situated at a lower temperature: $T_g = -43$ °C. In their work, Avérous et al. [14], observed the glass transition at $T_g = -50$ °C.

Furthermore, the T_g values obtained by DMA are not exactly the same as those given by DSC. Such discrepancies have been reported and discussed by many authors for various polymeric systems [14]. They are ascribed to the kinetic nature of the glass transition, the heating rate and loading frequency utilized in DSC and DMA experiments being different in terms of molecular mobility. The influence of time on viscoelastic response is verified from DMA tests performed at four frequencies ($f = 1$, 2.5, 10, and 25 Hz). The curves displayed in Fig. 7 show that, for both materials, the loss peak is shifted by about 2 °C when frequency is increased from 1 to 25 Hz. Influence of frequency on the glass transition has been modeled by some authors [18] in terms of the Arrhenius activation law: $f = f_0 \exp(-E_a/RT)$. The apparent

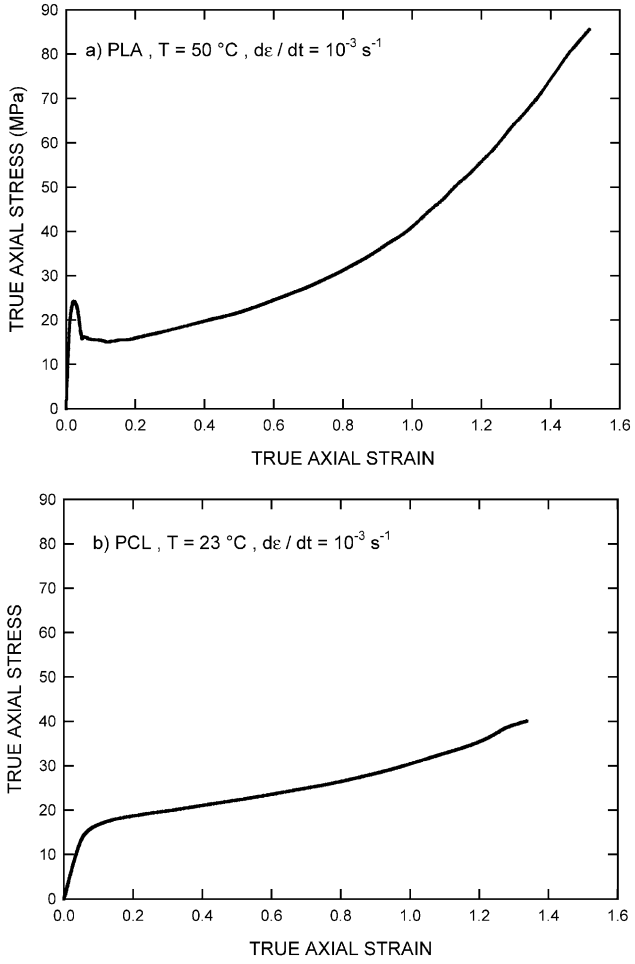

Fig. 9. True stress/true strain curves for (a) PLA at 50 °C and (b) PCL at 23 °C.

activation energy, E_a, equal to the slope of the ln(f) vs. $1/T_g$ curves, is equal to 255 kJ/mol for PLA and to 105 kJ/mol for PCL (Fig. 8).

4. Plastic deformation and strain-induced damage

4.1. Stress–strain behavior and volume changes at constant true strain rate

The constitutive behavior of PLA and PCL is shown in Fig. 9 by the true axial stress–strain curves obtained under uniaxial tension for a true axial strain rate $d\varepsilon_{33}/dt = 10^{-3}\ s^{-1}$. In order to ensure sufficient stretch before rupture for both polymers, the tests were performed: (i) for PLA at 50 °C, that is slightly below glass transition temperature and, (ii) for PCL at 23 °C, well above glass transition.

At 50 °C the behavior of PLA (Fig. 9(a)) is typical of a glassy polymer. The initial Young's modulus, $E=$ 2400 MPa, is characteristic of the stiffness of van der Waals bonds. At the end of the viscoelastic stage, the sharp yield point at $\sigma_{33}^{y} = 25$ MPa, is followed by a relatively high stress drop of about 7 MPa. This phenomenon corresponds here to an intrinsic strain-induced softening of the polymeric glass. It has nothing to do with the necking process that begins to develop in the same strain range, since the decrease of cross-section at the neck is already taken into account in the definition of true stress. After the yield drop is stabilized, a long plastic stage is observed. Like in many glassy polymers (e.g. poly(vinyl chloride) [19]), this stage begins as a quasi-horizontal plateau and then shows increasing strain hardening. Ultimately, it continues until the specimen reaches a true stress $\sigma_{33} = 80$ MPa at a true strain $\varepsilon_{33} = 1.5$. This ultimate true strain attained by PLA corresponds to a stretching ratio: $\lambda = 4.5$.

The true stress–true strain curve exhibited by PCL at 23 °C, shown in Fig. 9(b), is significantly different to that of PLA. Firstly, the much lower Young's modulus, $E=$ 300 MPa, results from the combination of rubber-like amorphous zones and more rigid crystallites. Subsequently, the yield point is rounded off, showing a progressive transition from the elastic stage to the plastic stage. This is similar to the tensile behavior of low-density polyethylene (LDPE) at room temperature [20]. Like for LDPE, the yield stress is better defined from the intersection of straight lines extrapolated from the elastic and plastic stages, respectively. Following this definition, one finds: $\sigma_{33}^{y} = 15$ MPa. It is noted that PCL does not exhibit strain softening at all. Instead, true stress shows continuous increase after yielding, with a progressively increasing strain hardening. The maximum true strain attained by PCL is $\varepsilon_{33} = 1.35$ (that is $\lambda = 3.85$) for a stress of $\sigma_{33} = 40$ MPa.

We will now focus our attention on the volume changes recorded in the course of the tensile tests presented above (Fig. 10). This novel functionality of the VidéoTraction© system is exploited in view of understanding the microstructural damage undergone by these special polymers under stretching.

The graph in Fig. 10(a) shows the evolution of volume strain vs. true axial strain for PLA. It is evident that the polymer experiences significant volume change on stretching. In the elastic stage, volume strain corresponds to the reversible dilatation under the effect of the hydrostatic stress, $\sigma_h = \sigma_{33}/3$. As such, one gets $\varepsilon_v = (1-2\nu)\varepsilon_{33}$, where ν is the Poisson's ratio, equal to 0.42 in present conditions. After the yield point is passed, volume strain increase shows a transient saturation in the strain range up to $\varepsilon_{33} \approx 0.1$, before resuming dramatically in the rest of the plastic stage. On the overall, the volume strain rate is nearly constant, ε_v reaching a maximal value of 0.27, when $\varepsilon \approx 1.4$ at the end of the test. Lastly, we consider, by supposing that the damage processes are isotropic, that the three components of volume strain tensor are equal ($\varepsilon_{11}^{v} = \varepsilon_{22}^{v} = \varepsilon_{33}^{v}$) and consequently that $\varepsilon_v = 3\varepsilon_{33}^{v}$.

Since, axial dilatation is one third of the volume dilatation, one can thus consider that damage processes participate by about 6.5% to the overall elongation of the polymer (0.065 = 0.27/3/1.4).

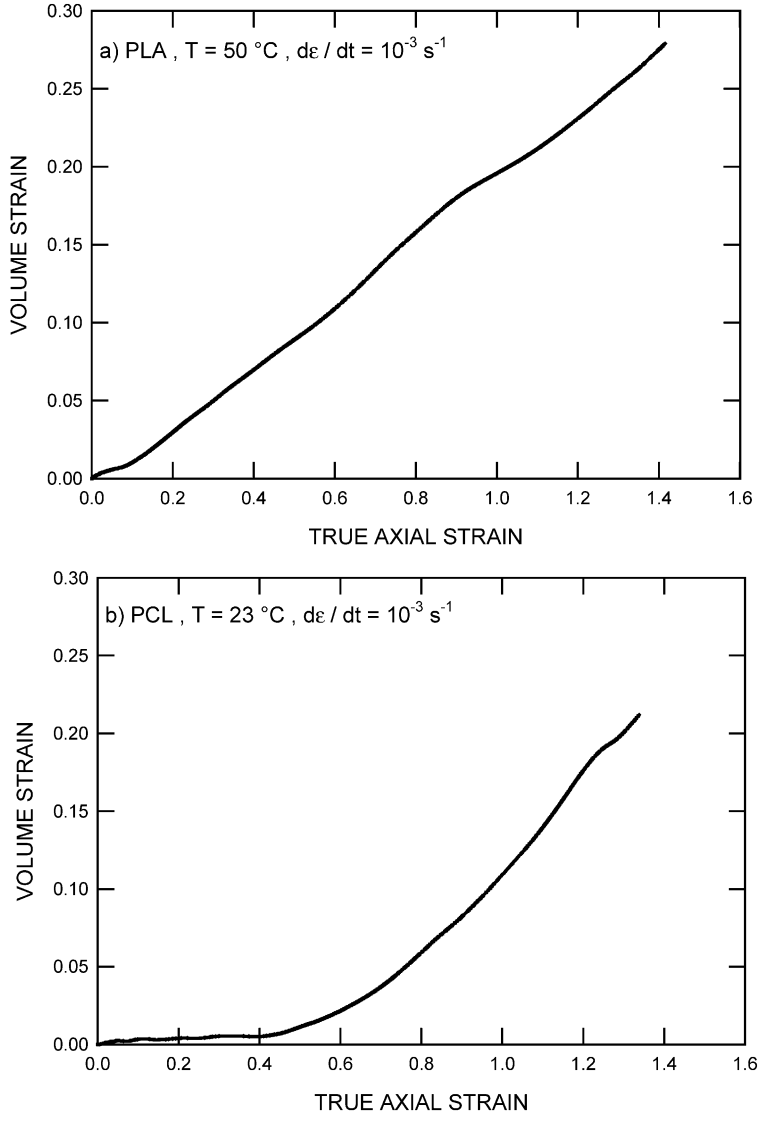

Fig. 10. Volume strain/true strain curves for (a) PLA at 50 °C and (b) PCL at 23 °C.

The evolution of volume strain in PCL under tension is displayed in Fig. 10(b). Also, in the elastic stage, the dilatation is related to the Poisson's ratio. In this polymer, this parameter is higher, $\nu \approx 0.47$, so that ε_v remains lower than 0.005 for a while. As such, this semi-crystalline polymer with a rubberlike amorphous phase can be considered to be nearly incompressible at moderate plastic strains. However, at larger strains, a dramatic upturn of the ε_v vs. ε_{33} is observed. It starts at a strain of about 0.4 and rapidly increases, even at an accelerated rate above $\varepsilon_{33} = 0.7$. Eventually, when the material reaches its maximal strain at $\varepsilon \approx 1.3$, volume strain is as large as $\varepsilon_v \approx 0.2$, nearly as much as for PLA. Here, for PCL it is found that the deformation supported by the cavitation mechanisms represents more than 5% of the total deformation.

4.2. Effects of the strain rate

The experimental results displayed in Figs. 11 and 12 show the effect of true strain rate ($\dot{\varepsilon}_{33} = 5 \times 10^{-3}$, 10^{-3} and 10^{-4} s^{-1}) on the stress–strain response of PLA and PCL, respectively. Like above, the testing temperature is 50 °C for PLA and 23 °C for PCL. Both polymers exhibit significant strain-rate sensitivity, the general tendency being an increase of flow stress and volume strain with strain rate. However, this general rule suffers some exceptions.

Concerning PLA, yield stress is much more sensitive to strain rate than the steady-state plastic stress. In terms of strain-rate sensitivity, $m = [\partial \ln \sigma_{33} / \partial \ln \dot{\varepsilon}_{33}]_{\varepsilon_{33}}$, one get $m = 0.28$ at yield and only $m = 0.12$ in the plateau at $\varepsilon = 0.2$. The higher strain-rate dependence of yield stress for glassy

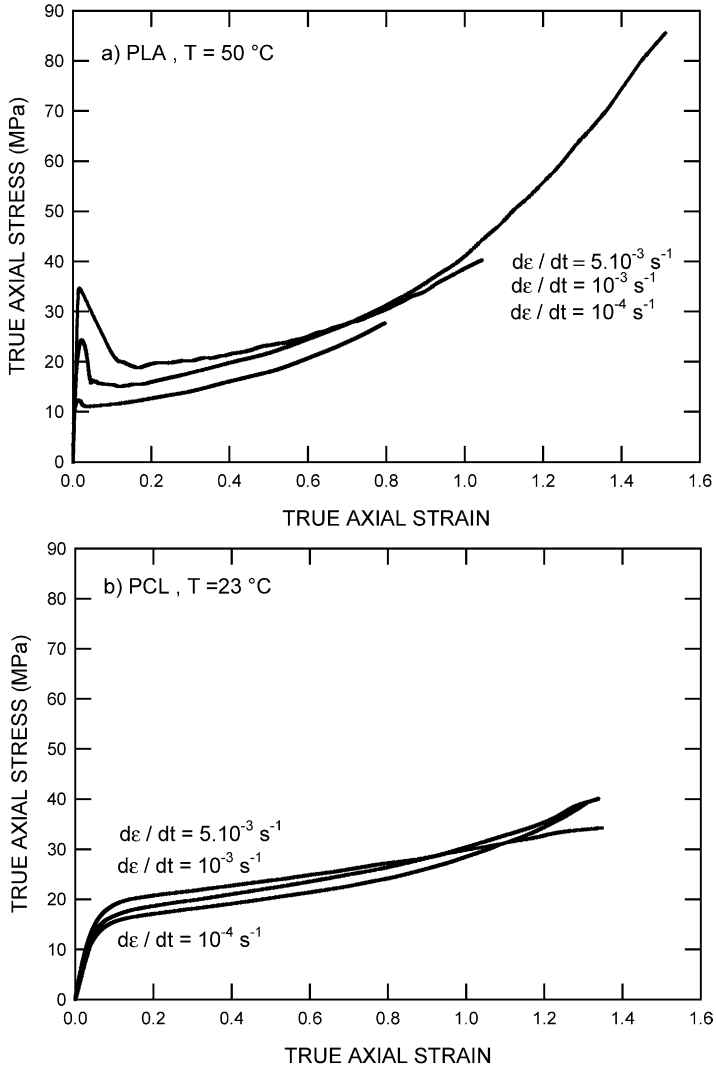

Fig. 11. True stress/true strain curves for different strain rates for (a) PLA at 50 °C and (b) PCL at 23 °C.

polymers is not new. One of the authors (G'Sell) has already observed this phenomenon in the case of PVC [19] and interpreted it in terms of the kinetic nature of the yield process: since the peak stress corresponds to the onset of shear defect multiplication, it increases dramatically with strain rate, while the steady-state regime, which results in a balance between defect formation and elimination, shows only a moderate increase. Later, in the ultimate regime, one can remark 'anomalous' strain-rate sensitivity for the two fastest experiments. Although the curve at $5\times10^{-3}\,s^{-1}$ is higher than the one at $10^{-3}\,s^{-1}$ at yield and at the very beginning of the steady-state plastic range, it shows a downward inflexion at larger strain and eventually passes below the latter for strains higher than 0.7. This phenomenon has been often observed by previous authors but rarely explained with correct arguments. Thanks to the simultaneous characterization of volume strain in the experiments presented here, we are now capable to give a definite explanation to this negative strain-rate sensitivity. Analysis of volume strain curves of PLA (Fig. 12(a)) show that plastic damage is also sensitive to strain-rate, especially at large strains. For example, at $\varepsilon\approx1.0$, one notes that the curve at $5\times10^{-3}\,s^{-1}$ exceeds that at $10^{-3}\,s^{-1}$ by more than 10%. This result indicates that damage mechanisms are more active at fast strain rates. Whatever the exact nature of these mechanisms, larger volume strain implies larger concentration of voids in the microstructure, and consequently weaker tensile response. Quantitative treatment of this factor will be the object of a forthcoming paper.

The results obtained with PCL are somewhat different as those presented above, for what is concerned with the initiation of plasticity. Since, this polymer does not show any yield drop, strain-rate sensitivity concerns directly the steady-state plastic regime for which m is relatively low, as we saw in Section 4.1. Later, at strains higher than 0.9, the same negative strain-rate sensitivity is observed, the stress–strain curve at $5\times10^{-3}\,s^{-1}$ crossing the curve at $10^{-3}\,s^{-1}$. Again, this is quantitatively interpreted by the strong influence of strain rate on damage.

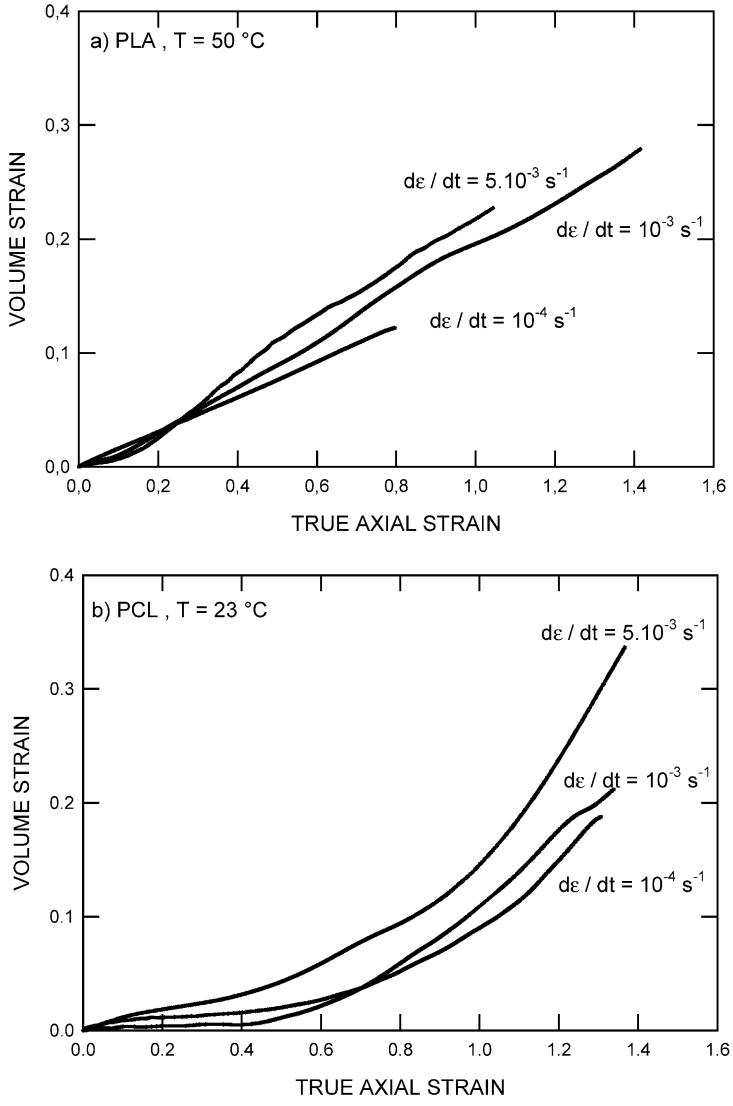

Fig. 12. Volume strain/true strain curves for different strain rates for (a) PLA at 50 °C and (b) PCL at 23 °C.

4.3. Assessment of volume strain by X-ray densitometry

The characterization of stretched specimens by X-ray densitometry is presented here in order to check with a different technique the volume strain measurements deduced from the VidéoTraction™ tests. The reduced intensity profiles, $\langle I(x_3)\rangle/I_0$ are displayed in Fig. 13 forth PLA and PCL samples deformed (in the RVE) up to $\varepsilon_v = 1$ and $\varepsilon_v = 1.4$, respectively. In this method, $\langle I(x_3)\rangle$ represents the average intensity across the specimen width at a given coordinate x_3. From these profiles, the distribution of volume strain in the material along the tensile axis is determined (Fig. 14). The maximum of the latter profile corresponds to the position of the RVE, so that the volume strain data obtained from VidéoTraction© and X-ray densitometry can be compared. However, for the former method, care was taken to determine volume strain after unloading and 3 h relaxation, since radiographic investigation is also performed at rest. Results summarized from both methods in Table 1 reveal that X-ray measurements systematically underestimate volume strain by comparison with VidéoTraction© data. It seems that this discrepancy is mainly due to the intrinsic uncertainty of radiographic analysis. As, such, it is seen in Fig. 14 that the ε_v vs. x_3

Table 1
Volume strain data determined for PLA and PCLfrom VidéoTraction™ and X-ray densitometry

	VidéoTraction© under load	VidéoTraction© 3 h after unloading	X-ray densitometry
PLA ($\varepsilon_{33}=1$)	$\varepsilon_v=0.21$	$\varepsilon_{vr}=0.19$	$\varepsilon_v=0.15$
PCL ($\varepsilon_{33}=1.4$)	$\varepsilon_v=0.19$	$\varepsilon_{vr}=0.17$	$\varepsilon_v=0.10$

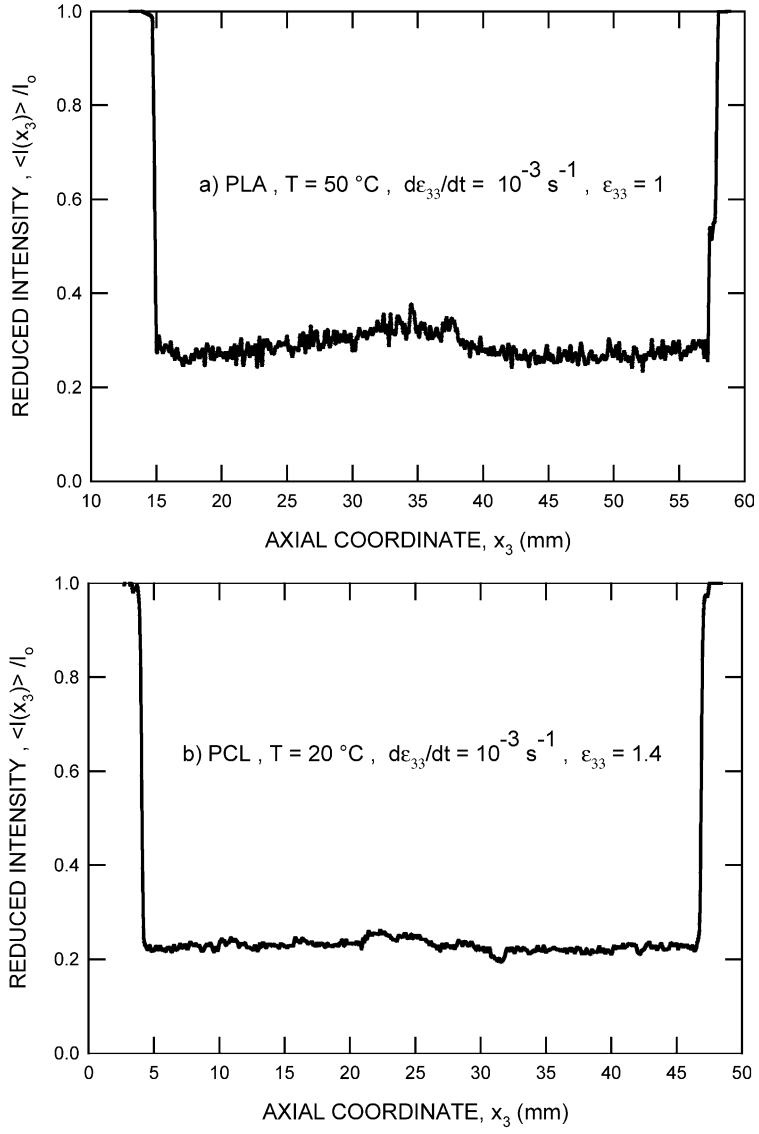

Fig. 13. X-ray densitometry profile for (a) PLA at $\varepsilon_{33}=1.0$ and (b) PCL at $\varepsilon_{33}=1.4$.

curves obtained with the latter method are very noisy, so that the accuracy for determining volume strain at the RVE is not better than 0.05. Further experimental effort is now in progress for completing the basic approach performed in Nancy with more sophisticated X-ray techniques including 3D micro-tomography.

Whatever the cause of experimental errors, it is important to notice that plastic damage in PLA after stretching at 50 °C is systematically smaller than in PCL stretched at 23 °C for the same extension ratio in the neck. Not only this property is shown by the tensile tests and by X-ray densitometry, but also it is revealed by the naked-eye observation. For example, photographs in Fig. 15 correspond to specimens deformed up to the same strain, $\varepsilon_{33}=1.0$, and subsequently unloaded. It is evident that PLA exhibits much more whitening than PCL. Since, this phenomenon is due to light diffusion from microscopic, the latter observation constitute a complementary evidence that deformation damage plays a more important role in PLA than in PCL, presumably because of the glassy nature of the amorphous matrix in the former polymer.

4.4. Microscopic characterization of cavitation mechanisms

For stretched PLA and PCL samples, the surface at the VER was investigated by scanning electron microscopy. Fig. 16(a) shows that PLA samples contain number of voids. Most of these defects exhibit an elliptical shape with major axis parallel to the tensile axis. As such, their transverse size is less than 5 μm while their length is sometimes more than 20 μm. They obviously correspond to cracks that were deformed during the rest of the test after their nucleation. Also many microscopic particles are observed in the vicinity

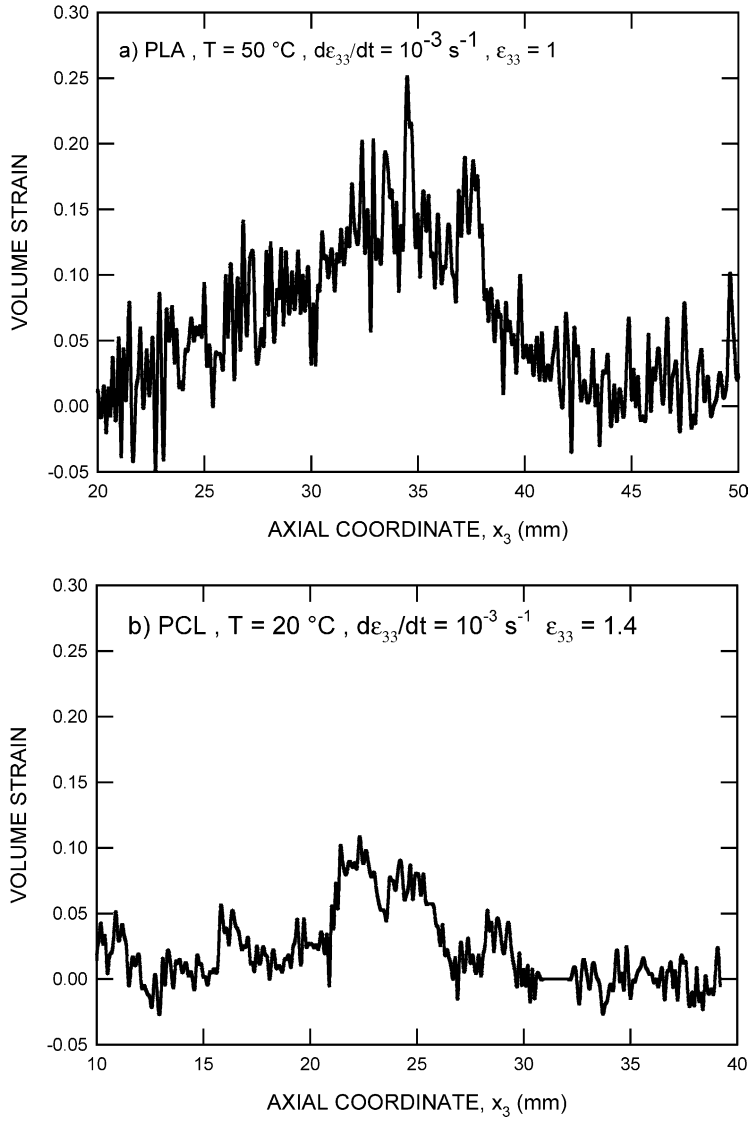

Fig. 14. Distribution of volume strain along tensile axis determined by X-ray densitometry for (a) PLA at 50 °C and (b) PCL at 23 °C.

of the voids which were presumably detached from the glassy matrix.

Unexpectedly, the damage process in PCL appears at the surface with a very different appearance. The micrograph in Fig. 16(b) does not show definite void, but rather a collection of grooves, about 0.5 μm in width, oriented along the tensile direction. Further investigation will definitely be necessary to explore more deeply the morphology of damage defects in PCL. However, since it was demonstrated above by VidéoTraction and radiography that cavitation represents nearly 18% of the total volume at that level of strain, the own features of PCL microstructure should play a specific role in this polymer, namely high crystallinity and rubber-like matrix. Presumably the amorphous matrix deforms without extensive cavitation in the first part of the plastic stage, up to an axial true strain of about 0.4. Following the arguments of Nitta and Takayanagi [21], one can envisage that this critical strain marks the beginning of crystallite fragmentation under the effect of lamellar bending. Consequently, the size of voids resulting from this damage mechanism is certainly similar to the crystallite size, of the order of 100 nm.

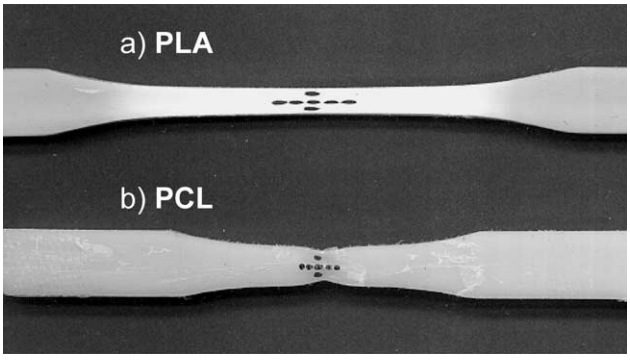

Fig. 15. Direct observation of samples stretched up to $\varepsilon_{33}=1.0$ and unloaded: (a) PLA at 50 °C and (b) PCL at 23 °C.

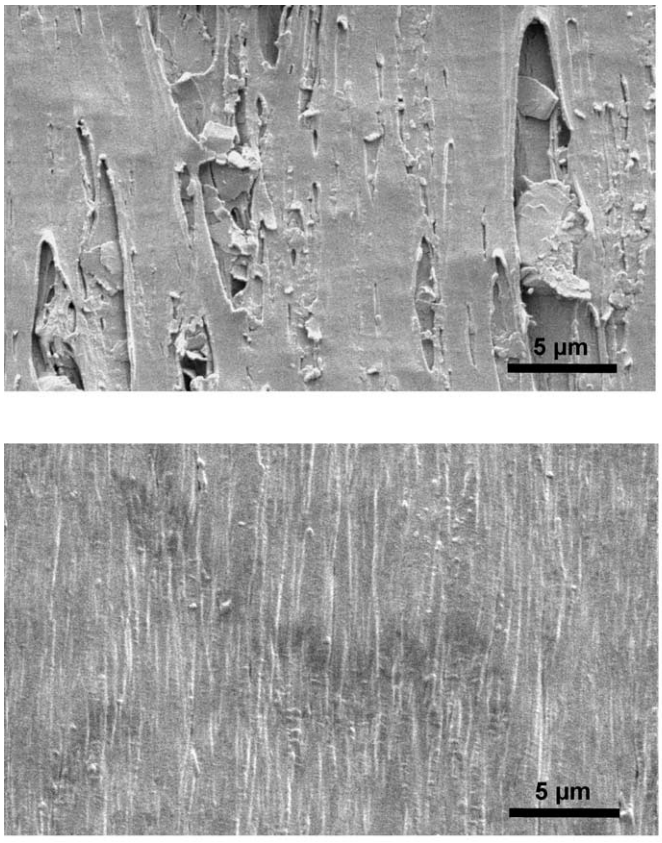

Fig. 16. Scanning electron micrograph of cavitation in the RVE of samples stretched up to $\varepsilon_{33} \approx 1.4$ (a) PLA at 50 °C and (b) PCL at 23 °C (tensile axis is vertical).

Later, they are likely to grow and coalescence during the last part of the plastic stage. At that point we have no definite interpretation of the groove geometry observed at the surface that should correspond to a high degree of elongation with no relationship with the applied deformation. To date, attempts to expose internal surfaces of deformed PCL samples in view of observing the void morphology in the core of the material were unsuccessful. This is because cutting and polishing operations 'spread' the rubber-like soft matrix over the preparation. Operating under cryogenic conditions is an alternative solution that will be tested in the future.

Other physical techniques are now in course of investigation in order to characterize the size and morphology of defects in PLA and PCL. The most promising ones concern the diffusion of gases and liquids in the void network produced by plastic deformation. Results and interpretation of these experiments will be the object of a forthcoming publication.

5. Conclusions

The microstructure and stretching behavior of two degradable polymers was investigated in this work: PLA with a controlled amount of D-isomer and PCL.

In its undeformed state, the injected PLA samples show little crystallinity (14.3 wt%), the morphology being characterized by orthorhombic crystallites embedded within an amorphous matrix that is glassy at room temperature. As for the PCL, its crystallinity is higher (53.1 wt%). The crystalline lamellae are also orthorhombic but the amorphous phase is rubbery at ambient temperature.

Although very brittle at room temperature, PLA shows extensive ductility at 50 °C. Like most glassy polymers, its tensile behavior is characterized by marked stress drop at yield followed by a steady-state plastic stage with progressive hardening. By means of a video multiaxial extensometer, it was possible to reveal that this polymer develops extensive damage in uniaxial tension, volume strain reaching 0.27 for an axial strain of 1.4.

Conversely, the PCL samples behave at 23 °C like most semi-crystallized polymers possessing a rubber-like matrix: yield point is quite progressive and strain hardening is limited. Damage is delayed in this polymer, starting at a strain of 0.5 only, but it eventually increases with a higher rate. As such, volume strain reaches 0.2 for an axial strain of 1.3.

X-ray densitometry, also utilized in this work, provides a semi-quantitative confirmation of the results of volume strain measurement.

SEM investigation was performed at the level of the

surface on tensile samples deformed at the same strain, $\varepsilon_{33} = 1.4$. The PLA specimens exhibit large voids highly elongated along the tensile direction. By contrast, the PCL specimens show no major voiding, presumably because of the rubbery nature of this polymer.

Acknowledgements

This work was performed in collaboration with Apollor-Union SA, which provided the PLA. The authors are indebted to Mr Laurent Plessis for assistance for injection molding the samples. They also acknowledge for the kindness of Dr H. Wautier, of Solvay Company, who supplied PCL. Thanks to all members of the LPM for help in completing the experiments. GPC characterization of the PLA samples was kindly performed by A. Janorkar (Clemson University, USA). Also this work was improved by valuable scientific discussion with Profs L. Avérous (Strasbourg, France) and M. Vert (Montpellier, France).

References

[1] Tjong SC, Xu Y, Meng YZ. Polymer 1999;40:3703–10.
[2] Broz ME, Vanderhart DL, Washburn NR. Biomaterials 2003;24:4181–90.
[3] Agarwal M, Koelling KW, Chalmers JJ. Biotechnol Prog 1998;14:517–26.
[4] Eldsäter C, Erlandsson B, Renstad R, Albertsson AC, Karlsson S. Polymer 2000;41:1297–304.
[5] Lijian L, Suming L, Gareau H, Vert M. Biomacromolecules 2000;1:350–9.
[6] Gonzalez MF, Ruseckaite RA, Cuadrado TR. J Appl Polym Sci 1999;71:1223–30.
[7] Wang L, Ma W, Gross RA, McCarthy SP. Polym Degrad Stab 1998;59:161–8.
[8] Lostocco MR, Huang SJ. Polym Degrad Stab 1998;61:225–30.
[9] Lunt J. Polym Degrad Stab 1998;59:145–52.
[10] Martin O, Avérous L. Polymer 2001;42:6209–19.
[11] Avella M, Errico ME, Laurienzo P, Martuscelli E, Raimo M, Rimedio R. Polymer 2000;41:3875–81.
[12] G'Sell C, Hiver JM, Dahoun A. Int J Sol Struct 2002;39:3857–72.
[13] Hoogsteen W, Postema AR, Pennings AJ, Brinke T, Zugenmaier P. Macromolecules 1990;23:634–42.
[14] Avérous L, Moro L, Dole P, Fringant C. Polymer 2000;41:4157–67.
[15] Kister G, Cassanas G, Vert M. Polymer 1998;39:267–73.
[16] Anderson KS, Lim SH, Hillmeyer MA. J Appl Polym Sci 2003;89:3757–68.
[17] Shichun J, Xiangling J, Lijia A, Bingzheng J. Polymer 2001;42:3901–7.
[18] Lopez-Manchado MA, Arroyo M. Polymer 2000;41:7761–7.
[19] G'Sell C, Jonas JJ. J Mater Sci 1981;16:1956–74.
[20] G'Sell C, Jonas JJ. J Mater Sci 1979;14:583–891.
[21] Nitta K-H, Takayanagi M. J Appl Polym Sci 2000;38:1037–44.